ACS Medicinal Chemistry Letters

Letter

pubs.acs.org/acsmedchemlett

Discovery of Potent and Simplified Piperidinone-Based Inhibitors of the MDM2−p53 Interaction

Ming Yu,*,† Yingcai Wang,† Jiang Zhu,† Michael D. Bartberger,§ Jude Canon,∥ Ada Chen,† David Chow,† John Eksterowicz,† Brian Fox,† Jiasheng Fu,† Michael Gribble,† Xin Huang,⊥ Zhihong Li,† Jiwen (Jim) Liu,† Mei-chu Lo,† Dustin McMinn,† Jonathan D. Oliner,∥ Tao Osgood,∥ Yosup Rew,† Anne Y. Saiki,∥ Paul Shaffer,⊥ Xuelei Yan,† Qiuping Ye,‡ Dongyin Yu,§ Xiaoning Zhao,† Jing Zhou,† Steven H. Olson,† Julio C. Medina,† and Daqing Sun*,†

†Departments of Therapeutic Discovery and ‡Pharmacokinetics and Drug Metabolism, Amgen Inc., 1120 Veterans Boulevard, South San Francisco, California 94080, United States

§Departments of Therapeutic Discovery and ∥Oncology Research, Amgen Inc., One Amgen Center Drive, Thousand Oaks, California 91320, United States

⊥Department of Therapeutic Discovery, Amgen Inc., 360 Binney Street, Cambridge, Massachusetts 02142, United States

Supporting Information

ABSTRACT: Continued optimization of the N-substituent in the piperidinone series provided potent piperidinone−pyridine inhibitors **6**, **7**, **14**, and **15** with improved pharmacokinetic properties in rats. Reducing structure complexity of the *N*-alkyl substituent led to the discovery of **23**, a potent and simplified inhibitor of MDM2. Compound **23** exhibits excellent pharmacokinetic properties and substantial in vivo antitumor activity in the SJSA-1 osteosarcoma xenograft mouse model.

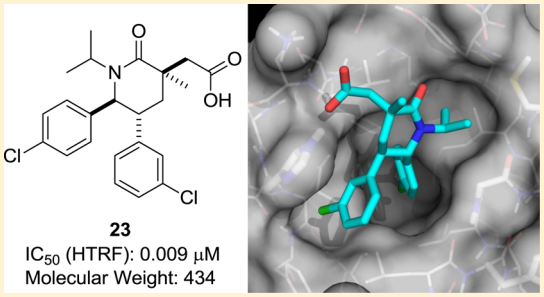

KEYWORDS: *MDM2, p53, protein−protein interaction, piperidinone, pyridine*

Protein p53 has been recognized as the "guardian of the genome" and is a main cell tumor suppressor.[1] It induces the cell growth arrest and apoptosis in response to DNA damage or stress.[2,3] In about 50% of human cancers, p53 is mutated or deleted resulting in loss of it functions. The wild-type p53 in the remaining 50% of malignancies is regulated by human murine double minute 2 (MDM2) oncoprotein[4,5] through three main mechanisms. First, MDM2 directly binds to and blocks the N-terminal transcriptional activation domain of p53. Second, MDM2 promotes export of p53 from the nucleus to the cytoplasm. Finally, MDM2 induces degradation of p53 via ubiquitination through its E3 ligase activity.[6] Since these mechanisms can be blocked by neutralizing the MDM2−p53 interaction, disrupting this interaction has emerged as a promising strategy to reactivate the p53 pathway.[7] To date, studies with small molecule MDM2 inhibitors have demonstrated complete tumor regression in vivo.[8−10] Several of these molecules have been tested in the clinic for the treatment of cancer.[11−14]

We previously reported the discovery of AM-8553 (**1**)[15] (Figure 1) as a potent and selective inhibitor of the MDM2−p53 interaction. Compound **1** substantially inhibited the MDM2−p53 interaction in the biochemical HTRF binding assay (IC_{50} = 1.1 nM) and the growth of human SJSA-1 tumor cell lines in the EdU cell proliferation assay (IC_{50} = 0.073 μM);[16] however, it suffered a high clearance (CL = 3.5 L/h/kg) and poor bioavailability (%*F* = 12) in mouse. The high potency of **1** can be rationalized by the cocrystal structure of **1** bound to MDM2.[15] Compound **1** occupies the three critical binding pockets of $Leu26_{(p53)}$, $Trp23_{(p53)}$, and $Phe19_{(p53)}$. The C5 aryl group reaches deep into the $Leu26_{(p53)}$ pocket and engages in a face-to-face π-stacking interaction with H96, while the C6 aryl group fills the $Trp23_{(p53)}$ binding cavity. The ethyl group is directed into the $Phe19_{(p53)}$ pocket by the conformational

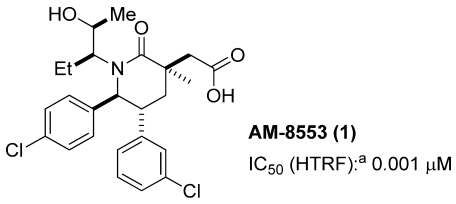

Figure 1. Chemical structure and potency of **1**. [a]IC_{50} in the HTRF binding assay.[16]

Received: April 8, 2014
Accepted: June 30, 2014
Published: June 30, 2014

constraint induced by the hydroxyethyl moiety. In addition, the carboxylate anion forms an electrostatic interaction with the imidazole on the H96 side chain of MDM2. Interestingly, the hydroxyl group in **1** is found to have no direct interaction with the protein but project toward the solvent. Analysis of the cocrystal structure suggested that the hydrophobic region adjacent to the Phe19 binding pocket and to the right of the *N*-alkyl group, might accommodate structure modifications. On the basis of this structure information, we conducted extensive modification of the *N*-alkyl substituent in **1**. These efforts led to the discovery of AMG 232, a new member of piperidinone MDM2 inhibitors. This compound is currently being evaluated in human clinical trials for the treatment of cancer.[10] In parallel to these efforts, an alternative strategy was pursued for the optimization of the *N*-alkyl substituent to improve metabolic stability and reduce structure complexity. In this article, we describe the continued optimization of the *N*-alkyl substituent, which led to the discovery of **23**, a potent and simplified MDM2 inhibitor with improved pharmacokinetic properties in rodents and excellent in vivo efficacy in the SJSA-1 osteosarcoma xenograft mouse model as well.

The optimization of the *N*-alkyl substituent began with methylation of the secondary alcohol in **1**. The resultant compound **2** (Table 1) exhibited similar potency (HTRF IC_{50} = 0.002 μM) as the parent **1** in the biochemical assay. Expanding the methoxy to a tetrahydrofuran (THF) produced compound **3**, which was slightly more potent (HTRF IC_{50} = 0.001 μM) than **2** in both biochemical and cell-based EdU assays, suggesting that the region occupied by the hydroxyethyl element of **1** might accommodate structural diversity (Figure 2). Inspired by tolerance of the THF ring in the region, we started to search for a heterocycle as a THF replacement in aim to eliminate the associated chirality and to improve potency.

The optimization of the *N*-alkyl substituent began with methylation of the secondary alcohol in **1**. The resultant compound **2** (Table 1) exhibited a similar potency (HTRF IC_{50} = 0.002 μM) as the parent **1** in the biochemical assay. Expanding the methoxy to a tetrahydrofuran (THF) produced compound **3**, which was slightly more potent (IC_{50} = 0.001 μM) than **2** in both biochemical and cell-based EdU assays, suggesting that the region occupied by the hydroxyethyl element of **1** might accommodate structural diversity. Inspired by tolerance of the THF ring in the region, we started to search for a heterocycle as a THF replacement in aim to eliminate the associated chirality and improve potency.

As summarized in Table 1, a small group of 5- or 6-membered heterocycles were explored. The oxazole **4** was considerably less potent than **3** in both biochemical and cell-based EdU assays, along with a high clearance of 5.7 L/h/kg in rats. However, compound **5** with a less polar thiazole had a maintained potency and a significantly low in vivo clearance in rats (CL = 0.39 L/h/kg). Encouraged by the improved in vivo metabolic stability of **5** in rats, we set out to optimize the polarity around the heterocycles. This SAR campaign led to the discovery of 2-pyridyl compound **6**, which had an IC_{50} of 0.003 μM in the biochemical assay and a reduced potency shift (9-fold) in the presence of human serum, as well as an IC_{50} of 0.43 μM in the cell-based EdU assay. Also of note is the fact that the ostensible zwitterionic character of **6** did not seem to impair its cellular permeability. This molecule was determined to have low in vitro intrinsic clearance of 13.0 and 7.0 μL/min/10^6 cells in rat and human hepatocyctes, respectively. Moreover, compound **6** demonstrated excellent in vivo PK properties (CL = 0.23 L/h/kg, $t_{1/2}$ = 3.5 h, and %*F* = 79) in rats. The 2-pyrimidyl analogue **7** exhibited a potency (IC_{50} = 0.42 μM)

Table 1. Heterocycle Piperidinone Derivatives

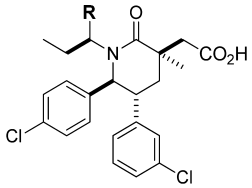

Compd	R	Potency (IC_{50}, μM)[a,b] HTRF (-) HS[c] (+) HS[d]	Cellular EdU[e] 10%HS[c]	Rat CL[f] (iv, L/h/kg)
1		0.001 0.006	0.073	2.1
2		0.002 0.016	0.143	ND[g]
3		0.001 0.020	0.123	1.7
4		0.008 0.036	0.84	5.7
5		0.006 0.066	1.10	0.39
6		0.003 0.028	0.43	0.28
7		0.007 0.050	0.42	0.77
8	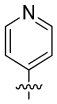	0.009 0.031	0.46	5.5
9		0.015 0.085	0.98	ND[g]

[a]Values were the means of more than two determinations; standard deviation was ±30%. [b]See ref 16 for assay protocols. [c]HS = human serum. [d]In the presence of 15% human serum. [e]SJSA-1 cell line. [f]Dosed iv: 0.5 mg/kg. [g]Not determined.

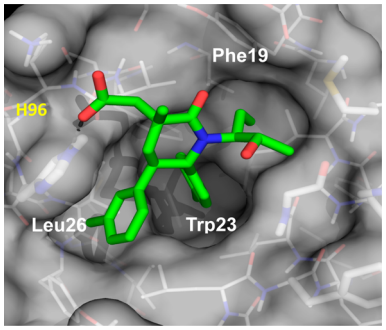

Figure 2. Cocrystal structure of **1** bound to human MDM2 (17−111) at 2.0 Å resolution. White labels indicate positions normally occupied by key p53 residues. H96 is labeled in yellow. PDB code: 4ERF.

comparable to **6** in the cellular EdU assay and reasonable in vivo PK properties in rats (CL = 0.77 L/h/kg). Analogues with the nitrogen atom located at distal positions (**8** and **9**) maintained potency but yielded no improvement in the in vivo clearance in rats.

With the 2-pyridine identified as the key feature for high inhibition and good PK properties, numerous pyridine derivatives were synthesized to define the alkyl group in the Phe19(p53) pocket. As listed in Table 2, the methyl compound

Table 2. Modifications for the Phe19$_{(p53)}$ Pocket

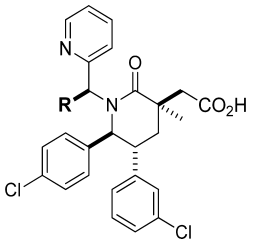

compd	R	potency (IC_{50}, μM)[a,b] HTRF (−) HS[c] (+) HS[d]	cellular EdU[e] 10%HS[c]
6	Et	0.003	0.43
		0.028	
10	Me	0.010	0.42
		0.062	
11	^{i}Pr	0.002	0.29
		0.025	
12	^{c}Pr	0.002	0.68
		0.019	
13	^{n}Pr	0.006	0.99
		0.092	

[a]Values were the means of more than two determinations; standard deviation was ±30%. [b]See ref 16 for assay protocols. [c]HS = human serum. [d]In the presence of 15% human serum. [e]SJSA-1 cell line.

10 was 2-fold less potent (IC_{50} = 0.010 μM) than **6** in the biochemical assays but equally active in the cellular EdU assay (IC_{50} = 0.42 μM). Expanding the ethyl group to an isopropyl group (**11**) marginally improved the biochemical (IC_{50} = 0.002 μM) and cellular potencies (IC_{50} = 0.29 μM). Utilizing cyclopropyl group at this position (**12**) led to no obvious improvement in the intrinsic potency but slight decrease in cellular activity (IC_{50} = 0.68 μM in the EdU assay). As exemplified by **13**, larger substituents were generally well tolerated but yielded no noticeable benefit. Overall, this set of compounds maintained high metabolic stability and generally exhibited desirable in vivo PK profiles in rats (e.g., CL = 0.20 L/h/kg and $t_{1/2}$ = 6.9 h for **13**).

To further optimize the binding affinity of **6** to MDM2, we explored a wide range of substitutions for the 2-pyridyl component in **6**. As shown in Table 3, compound **14**, featuring 6-methyl substitution, was equipotent to **6** in both biochemical (IC_{50} = 0.002 μM) and cellular EdU assays (IC_{50} = 0.28 μM) and had a moderate in vivo clearance of 0.93 L/h/kg in rats. Changing the methyl group (**14**) to a chlorine (**15**) at the 6-position resulted in a noticeable improvement of the intrinsic potency (IC_{50} = 0.0007 μM). However, this advantage was not well preserved in the human serum presented biochemical assay (IC_{50} = 0.023 μM) or the cell-based EdU assay (IC_{50} = 0.21 μM). Increasing the size of the 6-substituent, as exemplified by

Table 3. Fine Modification of the 2-Pyridyl Ring

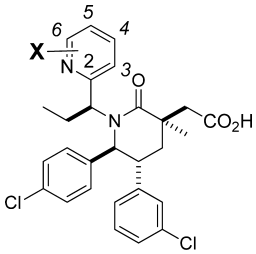

compd	X	potency (IC_{50}, μM)[a,b] HTRF (−) HS[c] (+) HS[d]	cellular EdU[e] 10%HS[c]	rat CL[f] (iv, L/h/kg)
6	H	0.003	0.43	0.23
		0.028		
14	6-Me	0.002	0.28	0.93
		0.032		
15	6-Cl	0.0007	0.21	1.2
		0.023		
16	6-^{c}Pr	0.005	1.82	ND[g]
		0.228		
17	5-Me	0.007	0.90	ND[g]
		0.123		
18	4-Me	0.006	0.89	ND[g]
		0.060		
19	3-Me	0.005	0.31	ND[g]
		0.183		

[a]Values were the means of more than two determinations; standard deviation was ±30%. [b]See ref 16 for assay protocols. [c]HS = human serum. [d]In the presence of 15% human serum. [e]SJSA-1 cell line. [f]Dosed iv: 0.5 mg/kg. [g]Not determined.

16 (X = 6-cPr), led to a potency decrease (IC_{50} = 0.005 μM). Finally, compounds **17**−**19** illustrated our attempts at the other positions of the ring as well. Overall, small groups were tolerated at these positions but offered no advantage over **6**.

The cocrystal structure of **16** bound to MDM2 was obtained by X-ray crystallography to a resolution of 1.7 Å (Figure 3).[17] Compound **16** binds to MDM2 in the similar fashion as

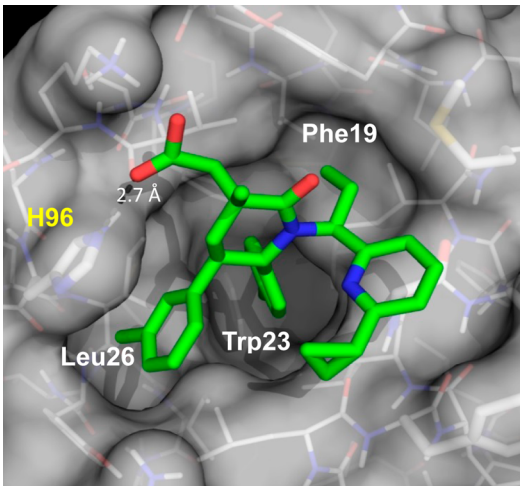

Figure 3. Cocrystal structure of **16** bound to human MDM2 (17−111) at 1.7 Å resolution. White labels indicate positions normally occupied by key p53 residues. H96 is labeled in yellow. PDB code: 4QO4.

described for **1**, occupying the three critical hydrophobic binding pockets and engaging in interaction with H96 as well. The 3-chlorophenyl group fills the Leu26(p53) pocket and engages in a face-to-face π-stacking interaction with H96, the 4-chlorophenyl group occupies the Trp23(p53) binding cavity. In addition, the carboxylate of **16** interacts with the imidazole of the H96 side chain of MDM2. The cyclopropylpyridine of **16** binds to the shelf region between Phe55 and Gly58, with the cyclopropyl moiety settled at a distance of 3.9 Å from the *meta*-chloro phenyl group. Importantly, the pyridyl moiety directs the ethyl group into the Phe19(p53) pocket to maximize the hydrophobic contact.

While the explorations discussed so far had led to the identification of several potent piperidinone−pyridine inhibitors (e.g., **6**, **7**, **14**, and **15**) with decent in vivo PK properties in rats, unfortunately, these molecules were found metabolically unstable in mouse (e.g., iv, CL = 3.1 L/h/kg and $t_{1/2}$ = 1.9 h for **6**). Therefore, they were not suitable for further pharmacodynamic studies in the SJSA-1 tumor xenografted mouse model. To eliminate the potential metabolic liability, we decided to reduce the structural complexity of this class of MDM2 inhibitors. With the *N*-alkyl substituent being truncated into a 2-pyridyl ring (Table 4), the resulting compound **20** was 3-fold less potent (IC_{50} = 0.013 μM) than **6** in the serum-free biochemical assay. Switching the aromatic ring from 2-pyridyl to phenyl (**21**) resulted in a considerable improvement in binding affinity (HTRF IC_{50} = 0.004 μM). Also of note is that compound **21** was fairly comparable (IC_{50} = 0.055 μM) to **6** in the human serum mediated biochemical assay as well. These findings prompted us to further reduce the structure complexity of the *N*-alkyl substituent. Replacing the *N*-phenyl moiety in **21** with a *N*-3-pentyl or *N*-isopropyl group resulted in compounds **22** and **23**, which were as nearly potent as **6** in the serum-free biochemical assay and the cell-based EdU assay.[18] Furthermore, both **22** and **23** had a lower intrinsic clearance in rat hepatocytes (18.8 μL/min/10^6 cells for **22** and 8.5 μL/min/10^6 cells and **23**) as compared to **1** (21 μL/min/10^6 cells).

Table 4. Structure Simplicity-Driven Modifications

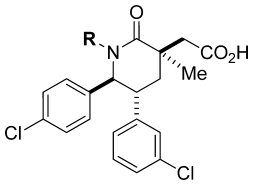

Compd	R	Potency (IC_{50}, μM)[a,b] HTRF (-) HS[c] (+) HS[d]	Cellular EdU[e] 10%HS[c]	Rat CL[f] (iv, L/h/kg)
6	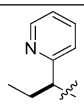	0.003 0.028	0.43	0.23
20		0.013 0.122	ND[g]	2.16
21		0.004 0.055	ND[g]	2.45
22		0.003 0.055	0.54	0.45
23		0.009 0.119	0.38	1.04

[a]Values were the means of more than two determinations; standard deviation was ±30%. [b]See ref 16 for assay protocols. [c]HS = human serum. [d]In the presence of 15% human serum. [e]SJSA-1 cell line. [f]Dosed iv: 0.5 mg/kg. [g]Not determined.

Consistent with their improved metabolic stability in rat hepatocytes, compounds **22** and **23** showed low in vivo clearance (0.45 and 1.04 L/h/kg for **22** and **23**, respectively) and good oral bioavailability (38% and 48% for **22** and **23**, respectively) in rats. Similarly, compounds **22** and **23** displayed a substantially lower clearance (0.99 and 1.03 L/h/kg for **22** and **23**, respectively) and higher oral exposure (42% for **22** and 32% for **23**) compared to **1** in the mouse.[19]

As a result of the cellular potency (EdU IC_{50} = 0.38 μM) and excellent oral exposure in mouse, a pharmacodynamic (PD) assay[20] with the SJSA-1 osteosarcoma tumor cells was used to assess the effects of **23** on the activation of p53 pathway. SJSA-1 tumor cells were implanted in mice 2 weeks prior to treatment. Compound **23** was orally administered at a single dose of 100 or 200 mg/kg, and p21 mRNA levels, a transcriptional target and pharmacodynamic readout for p53 activity, were measured over time, relative to the vehicle control. In this experiment, 14-fold induction of p21 over the vehicle was observed approximately 4 h after the 100 mg/kg of **23** was dosed orally, while the 200 mg/kg dose group achieved 15-fold p21 induction from 4 h postdose out to 8 h (Figure 4a). In a

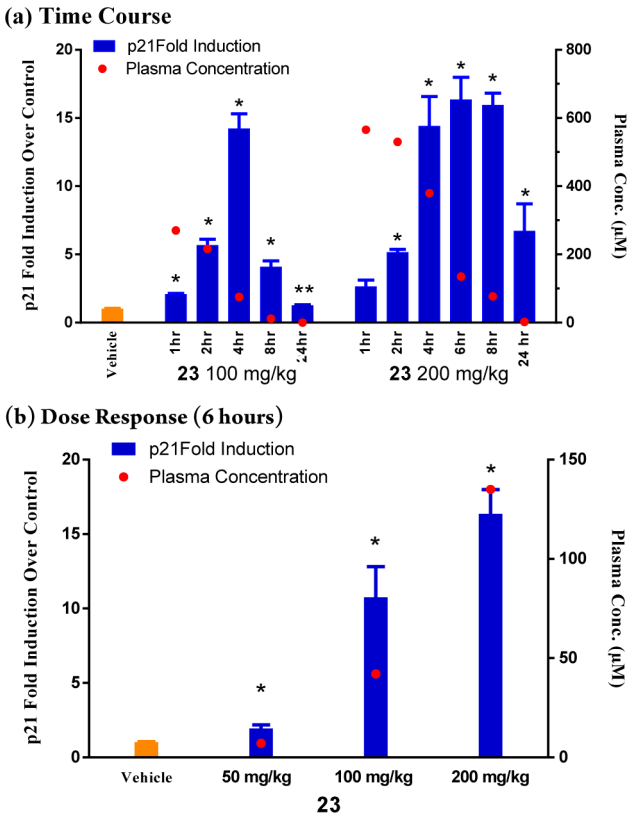

Figure 4. Pharmacodynamic study: treatment with **23** caused time- and dose-dependent induction of p21 mRNA in SJSA-1 tumor xenografts. *p < 0.05. (a) Vehicle and 100 or 200 mg/kg of **23** was administered orally once. (b) Vehicle and 50, 100, or 200 mg/kg of **23** was administered orally once.

parallel experiment, a dose-dependent increase in p21 mRNA induction was also observed (Figure 4b). These data confirm that compound **23** achieved an on-target activation of the p53 pathway and provided dose-selection guidance for the xenograft study. Similarly, a time- and dose-dependent increase in p21 mRNA induction was observed with **22** in this PD model (data not shown).

In the SJSA-1 osteosarcoma xenograft mouse model,[19] compound **23** substantially inhibited tumor growth at each designed dose compared to the vehicle (Figure 5). The 100 mg/kg QD and 50 mg/kg BID doses of **23** caused 96% and 82% tumor growth inhibition (TGI), respectively. Tumor regression was observed in the groups of 200 mg/kg QD and 100 mg/kg BID before animals were taken down due to severe body weight loss.

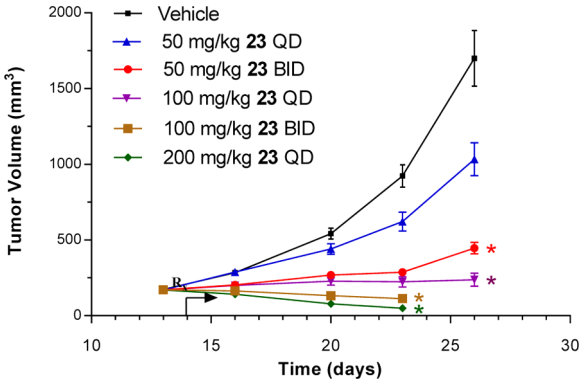

Figure 5. Treatment with **23** inhibited the growth of SJSA-1 tumors in vivo. $*p < 0.0001$. SJSA-1 cells (5 × 106) were implanted subcutaneously into female athymic nude mice. Treatment with vehicle or **23** at 50, 100, or 200 mg/kg QD or 50 or 100 mg/kg BID by oral gavage began on day 14 when tumors had reached ~200 mm^3 (n = 10/group). Tumor sizes were measured twice per week. Data represent mean tumor volumes, and the error bars represent SEM of data from 12 mice.

The synthetic procedures and characterization data for compounds **2**−**23** are provided in the Supporting Information.

In summary, continued optimization of the *N*-alkyl substituent in **1** led to the potent piperidinone−pyridine inhibitor **6** with excellent PK properties in rats. The cocrystal structure of pyridine analogue **16** bound to MDM2 confirmed the key interactions of the inhibitor with MDM2. Reducing structure complexity of the *N*-alkyl substituent led to the discovery of **23**, a potent and simplified inhibitor of MDM2. Compound **23** exhibited improved pharmacokinetic properties in mouse as compared to **1** and **6** and demonstrated substantial in vivo antitumor activity in the SJSA-1 osteosarcoma xenograft mouse model, albeit showing signs of toxicity at high doses in the efficacy study.

■ ASSOCIATED CONTENT

Supporting Information

(i) In vitro biological assays; (ii) in vivo study protocols; (iii) determination of cocrystal structures of **16** with MDM2; (iv) pharmacokinetic profiles of **1**, **22**, and **23** in rats and mouse; (v) synthetic experimental procedure and characterization data for compounds **2**−**23**. This material is available free of charge via the Internet at http://pubs.acs.org.

■ AUTHOR INFORMATION

Corresponding Authors

*(M.Y.) Tel: 650-244-2050. Fax: 650-837-9369. E-mail: yum@amgen.com.
*(D.S.) Tel: 650-244-2195. E-mail: daqings@amgen.com.

Notes

The authors declare no competing financial interest.

■ ACKNOWLEDGMENTS

We thank Dr. Iain Campuzano, Dr. Manuel Ventura, and Dhanashri Bagal for the acquisition of high resolution mass spectra.

■ REFERENCES

(1) Chen, J.; Wu, X.; Lin, J.; Levine, A. J. MDM2 inhibits the G1 arrest and apoptosis function of the p53 tumor suppressor protein. *Mol. Cell. Biol.* **1996**, *16*, 2445−2452.
(2) Vazquez, A.; Bond, E. E.; Levine, A. J.; Bond, G. L. The genetics of the p53 pathway, apoptosis and cancer therapy. *Nat. Rev. Drug Discovery* **2008**, *7*, 979−987.
(3) Chene, P. Inhibiting the p53-MDM2 interaction: An important target for cancer therapy. *Nat. Rev. Cancer.* **2003**, *3*, 102−109.
(4) Vogelstein, B.; Lane, D.; Levine, A. J. Surfing the p53 network. *Nature* **2000**, *408*, 307−310.
(5) Oliner, J. D.; Kinzler, K. W.; Meltzer, P. S.; George, D. L.; Vogelstein, B. *Nature* **1992**, *358*, 80−83.
(6) Wells, J. A.; McClendon, C. L. Reaching for high-hanging fruit in drug discovery at protein−protein interfaces. *Nature* **2007**, *450*, 1001−1009.
(7) Hainaut, P.; Hollstein, M. p53 and human cancer: the first ten thousand mutations. *Adv. Cancer Res.* **1999**, *77*, 81−137.
(8) Zhao, Y.; Yu, S.; Sun, W.; Liu, L.; Lu, J.; McEachern, D.; Shargary, S.; Bernard, D.; Li, X.; Zhao, T.; Zou, P.; Sun, D.; Wang, S. A potent small-molecule inhibitor of the MDM2−p53 interaction (MI-888) achieved complete and durable tumor regression in mice. *J. Med. Chem.* **2013**, *56*, 5553−5561.
(9) Ding, Q.; Zhang, Z.; Liu, J.-J.; Jiang, N.; Zhang, J.; Ross, T. M.; Chu, X.-J.; Bartkovitz, D.; Podlaski, F.; Janson, C.; Tovar, C.; Filipovic, Z. M.; Higgins, B.; Glenn, K.; Packman, K.; Vassilev, L. T.; Graves, B. Discovery of RG7388, a potent and selective p53−MDM2 inhibitor in clinical development. *J. Med. Chem.* **2013**, *56*, 5979−5983.
(10) Sun, D.; Li, Z.; Rew, Y.; Gribble, M.; Bartberger, M. D.; Beck, H. P.; Canon, J.; Chen, A.; Chen, X.; Chow, D.; Deignan, J.; Duquette, J.; Eksterowicz, J.; Fisher, B.; Fox, B. M.; Fu, J.; Gonzalez, A. Z.; Gonzalez-Lopez De Turiso, F.; Houze, J. B.; Huang, X.; Jiang, M.; Jin, L.; Kayser, F.; Liu, J.; Lo, M.; Long, A. M.; Lucas, B.; McGee, L. R.; McIntosh, J.; Mihalic, J.; Oliner, J. D.; Osgood, T.; Peterson, M. L.; Roveto, P.; Saiki, A. Y.; Shaffer, P.; Toteva, M.; Wang, Y.; Wang, Y. C.; Wortman, S.; Yakowec, P.; Yan, X.; Ye, Q.; Yu, D.; Yu, M.; Zhao, X.; Zhou, J.; Zhu, J.; Olson, S. H.; Medina, J. C. Discovery of AMG 232, a potent, selective, and orally bioavailable MDM2−p53 inhibitor in clinical development. *J. Med. Chem.* **2014**, *57*, 1454−1472.
(11) Information from www.clinicaltrials.gov. (a) RG7112 (Hoffmann-La Roche). (b) RG7388 (Hoffmann-La Roche). (c) SAR299155 (Sanofi). (d) MK-8242 (Merck). (e) AMG 232 (Amgen). (f) CGM-097 (Novartis). (g) DS-3032b (Daiichi Sankyo).
(12) Vu, B.; Wovkulich, P.; Pizzolato, G.; Lovey, A.; Ding, Q.; Jiang, N.; Liu, J. J.; Zhao, C.; Glenn, K.; Wen, Y.; Tovar, C.; Packman, K.; Vassilev, L. T.; Graves, B. Discovery of RG7112: A small-molecule MDM2 inhibitor in clinical development. *ACS Med. Chem. Lett.* **2013**, *4*, 466−469.
(13) Ding, Q.; Zhang, Z.; Liu, J. J.; Jiang, N.; Zhang, J.; Ross, T. M.; Chu, X. J.; Bartkovitz, D.; Podlaski, F.; Janson, C.; Tovar, C.; Zoran M. Filipovic, Z. M.; Higgins, B.; Glenn, K.; Packman, K.; Vassilev, L. T.; Graves, B. Discovery of RG7388, a potent and selective p53−MDM2 inhibitor in clinical development. *J. Med. Chem.* **2013**, *56*, 5979−5983.

(14) Carry, J.; Garcia-Echeverria, C. Inhibitors of the p53/hdm2 protein−protein interaction: path to the clinic. *Bioorg. Med. Chem. Lett.* **2013**, *23*, 2480−2485.
(15) Rew, Y.; Sun, D.; Gonzalez Lopez De Turiso, F.; Bartberger, M. D.; Beck, H. P.; Canon, J.; Chen, A.; Chow, D.; Deignan, J.; Fox, B. M.; Gustin, D.; Huang, X.; Jiang, M.; Jiao, X.; Jin, L.; Kayser, F.; Kopecky, D. J.; Li, Y.; Lo, M.; Long, A. M.; Michelsen, K.; Oliner, J. D.; Osgood, T.; Ragains, M.; Saiki, A. Y.; Schneider, S.; Toteva, M.; Yakowec, P.; Yan, X.; Ye, Q.; Yu, D.; Zhao, X.; Zhou, J.; Medina, J. C.; Olson, S. H. Structure-based design of novel inhibitors of the MDM2−p53 interaction. *J. Med. Chem.* **2012**, *55*, 4936−4954.
(16) Experimental details of in vitro assays can be found in the Supporting Information.
(17) The atomic coordinates are deposited in the Protein Data Bank under an accession code 4QO4.
(18) To evaluate p53 selectivity, we examine the effect of the piperidinone inhibitors on inhibiting the proliferation of HCT116 $p53^{wt}$ and $p53^{-/-}$ tumor cells in the BrdU assay. All of the piperidinone MDM2 inhibitors evaluated in the BrdU assay with HCT116 $p53^{wt}$ and $p53^{-/-}$ tumor cells display significant inhibition of cell proliferation in the $p53^{wt}$ tumor cells, but no inhibition in $p53^{-/-}$ tumor cells in concentrations up to 25 μM. For example, potency of **1** in wild-type p53 cells (IC_{50} = 0.20 μM) was substantially higher than that in p53 deficient cells (IC_{50} > 25 μM). No p53 selectivity data was collected for **23**.
(19) Detailed rat and mouse PK profiles can be found in the Supporting Information.
(20) Experimental details of in vivo studies can be found in the Supporting Information.